Dielectric response in ferroelectrics near polarization switching: analytical calculations, first-principles modeling and experimental verification

Sergiu Clima,[1*] Anne S. Verhulst,[1,2] Pratik Bagul,[2] Brecht Truijen,[1] Sean R.C. McMitchell,[1]
Ingrid De Wolf,[1,2] Geoffrey Pourtois,[1,3] Jan van Houdt,[1,2]
[1] imec, B-3001 Leuven, Belgium
[2] KU Leuven, B-3000 Leuven, Belgium
[3] University of Antwerp, B-2610 Antwerp, Belgium
* sergiu.clima@imec.be

Abstract — Ferroelectrics are increasingly used in nonvolatile memory applications. However, the impact of the electric dipole switching on its material parameters, in particular on the dielectric response, is not fully understood. In this work, an analytical model, linking the dielectric response to the potential energy curve, is first used to qualitatively illustrate the non-constant evolution of the dielectric response with applied electric field. Increasing precision, we then show from first-principles density-functional theory simulations that defect-free ferroelectric materials undergo changes in potential energy near the ferroelectric switching that lead to vibrational modes softening which impacts the dielectric response. In particular, we observe that the dielectric response ε of a ferroelectric material with anti-aligned polarization increases as the applied electric field increases towards the coercive field. We incorporate this new insight in the time-dependent NLS-based predictions and demonstrate that this evolution of the dielectric response right before polarization reversal is required for a proper match between experiment and prediction of the capacitance-voltage characteristics of the metal-ferroelectric-metal capacitor.

Index Terms—ferroelectricity, dielectric response.

I. Introduction

THE recent revival of technological interest in ferroelectric (FE) materials is due to the discovery of the CMOS-friendly HfO_2 class of FEs[1-6]. HfO_2-based FEs, which are fluorite-type FEs, solved one of the major drawbacks that was plaguing the classical perovskite FEs integration: scaling to relevantly small film thicknesses [7, 8]. The fluorite-type FEs have a larger bandgap and lower dielectric constant, hence higher electric fields, lower leakage currents and smaller FE film thickness can be achieved when scaling the FE devices [9-11].

To design scaled FEFET or MFM (metal-ferroelectric-metal) electronic devices [12-15], it is imperative to be able to accurately model the electrical behavior of such devices. The ultimate goal in terms of modeling is to have an all-physical calibrated model of the FE, including switching dynamics [16, 17]. For FEs, establishing such a model requires insight in the fundamental physics at the atomic scale. A so far not well-understood FE property is the capacitance-voltage (C-V) characteristic: it typically displays two peaks near the switching coercive fields (traces 2 and 4 in Fig. 1a, which are the curve sections between zero field and large positive or negative field, displaying switching behavior ("s") as indicated with a red arrow "s" for trace 2) and no peak for non-switching fields (traces 1 and 3 in Fig. 1a, which are the curve sections far enough beyond the coercive field (both positive and negative) and back to zero field, displaying no switching ("ns") as indicated with a blue arrow "ns" for the bottom trace 3).

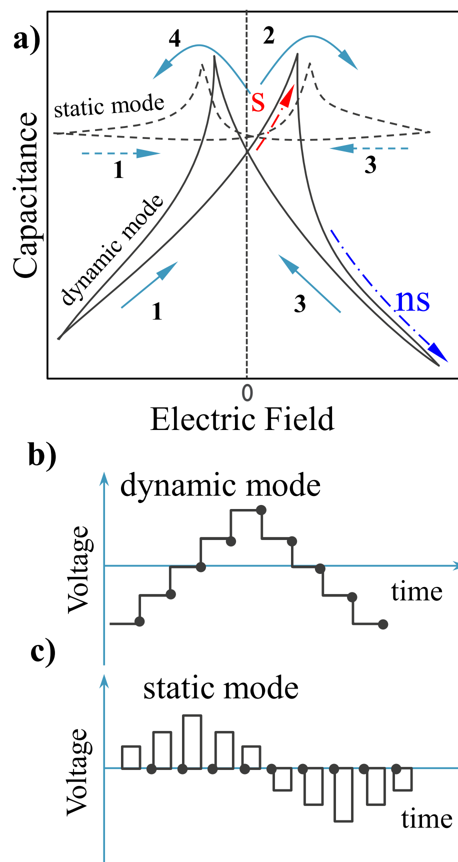

Fig. 1 a) Typical experimental C-V characteristics of a FE layer, measured in b) dynamic (full lines) and c) static (dashed lines) mode (adapted from ref [18]). The dots in b)-c) correspond to the time and DC voltage of a C-V measurement.

However, as can be seen in Fig. 1a, there are significant differences when the capacitance is measured under finite

© 2022 IEEE. Personal use of this material is permitted. Permission from IEEE must be obtained for all other uses, in any current or future media, including reprinting/republishing this material for advertising or promotional purposes, creating new collective works, for resale or redistribution to servers or lists, or reuse of any copyrighted component of this work in other works. https://doi.org/10.1109/TED.2022.3194822

electric field (dynamic mode Fig. 1b) or without any fixed electric field (static mode Fig. 1c) [18]. These differences are interpreted with various microscopic mechanisms, ranging from structural defects [18] to ferroelectric domain dynamics (reversible domain wall displacement [19]).

In this work, we infer from an analytical model, linking a simple potential energy representation of the electric dipole to its dielectric response (Section IIIB), that the dielectric response of the material (and therefore the capacitance) has a strong dependence on the applied electric field and the polarization direction with respect to the applied field. We confirm these findings with first-principles DFT (Density Functional Theory) simulations providing a more quantitative assessment of the dielectric response of a prototype $BaTiO_3$ FE material (Section IIIC). Finally, we are able to match the experimentally measured C-V curves of $BaTiO_3$ with an extended NLS model that takes this variable dielectric response into account (Section IIID).

II. Methodology

The first-principles DFT simulations are performed with CP2K [20] and are employing Goedecker-Teter-Hutter pseudopotentials [21], mixed with a double-zeta-valence-polarization (DZVP) localized basis set and a Perdew-Burke-Ernzerhof (PBE) functional [22]. The FE materials under study are rhombohedral (r-) and tetragonal (t-) $BaTiO_3$. The evolution of the phonon modes, and therefore the dielectric response, with the applied electric field is monitored. To compute the phonons and the dielectric response, we employ the modern theory of polarization in the frozen-phonon approximation.[23-26] In particular, a periodic 3×3×3 supercell is relaxed under various electric fields, until the atomic forces are relaxed below 10^{-4} Ha/Bohr, while the cell parameters are relaxed until the pressure drops below 100 bar. For every optimized-under-electric-field structure, we apply finite displacement perturbation on the atoms to compute the Born effective charges and atomic forces. The latter are diagonalized to obtain the phonon modes and frequencies, that are used to compute the ionic dielectric tensor (see Section IIIA).[27, 28]

For the experimental data, a sample is used consisting of a 50 nm $BaTiO_3$ film, grown with a Solmates 200 mm Pulsed Laser Deposition system (KrF excimer laser) on a $LaNiO_3$ substrate. The $BaTiO_3$ films are deposited with a laser fluence of 0.8 J/cm^2, a laser frequency of 66 Hz, and with the incident laser beam rastered across the diameter of the rotating ceramic target. The deposition is carried out in an oxygen ambient at a partial pressure of 0.20 mbar and with the substrate heated to 750°C. After the deposition, the films are cooled down under 0.10 mbar of oxygen atmosphere. Pt electrodes are deposited on top after which the capacitance-voltage (C-V) characteristics and polarization-electric field (P-E) hysteresis curves are measured with an aixACCT TF Analyzer 2000 measurement system.

III. Results and Discussion

A. The dielectric response

The material property that determines the measured capacitance C is the dielectric response ε, as reflected in C=$\varepsilon \cdot$*FormFactor,* with ε the permittivity (dielectric response) and *FormFactor* a material-independent design parameter (e.g. area/thickness). As an approximation, we can consider the dielectric response as consisting of paraelectric (PE) and FE dipole switching contributions:

$$\varepsilon = \varepsilon_{PE} + \frac{\partial P_S}{\partial E} \quad (1)$$

with P_S the spontaneous polarization (FE dipole) and E the electric field. The abrupt switching of the FE dipole (2nd term in Eq. (1)) is not included in the analysis. Since it is irreversible (one-time event), in experimental C-V measurements, it will only show up as a current spike for each dipole which is switching during the measurement. Given the small amplitude of the ac voltage, we have neglected this contribution in our analysis. Also in the analytical model (Section III.B) and in the first-principles dielectric response calculations, the 2nd term is not present. In what follows, we show that ε_{PE} is changing under applied electric field, contrary to its constant value in dielectric materials.

From first-principles, the ionic (atomic vibrational) component of the dielectric response tensor, which is expected to have the largest contribution (larger than the electronic component), is computed as follows [28]:

$$\varepsilon_{atom}^{ab} = \frac{4\pi e^2}{\Omega}\sum_{\lambda}\frac{Z_{\lambda a}Z_{\lambda b}}{\omega_{\lambda}^2}, \quad (2)$$

where *a,b* are displacement and field directions, Ω is the unit cell volume, e is the electron charge, λ counts over the vibrational modes, $Z_{\lambda a/b}$ is the vibrational mode polarizability, and ω is the vibrational mode frequency.

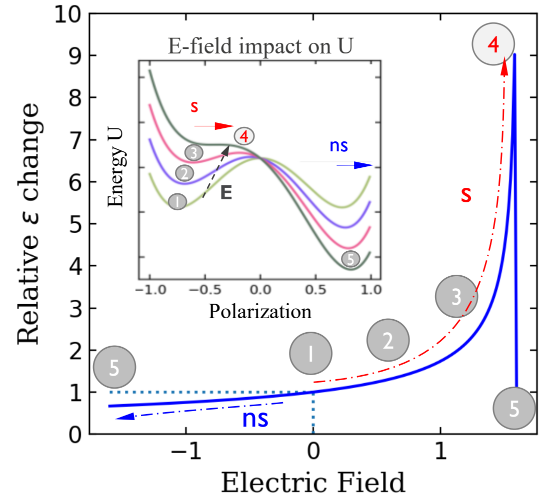

Fig. 2. Qualitative evolution of the dielectric response of the electric dipole with the applied electric field (relative to its value without applied electric field), as derived for a hypothetical material from the potential energy curvature (Eq. (3)) before switching (labels 1,2,3) at switching (label 4) and after polarization switching (label 5). The inset shows the corresponding potential energy curves versus polarization for the considered electric fields.

B. Analytical model

From Eq. (2), we observe the following qualitative dielectric response proportionality: $\varepsilon \sim 1/\omega^2$. The contribution of the spontaneous polarization to ε (1st term in Eq. (1)) will therefore depend on the atomic vibrational mode frequency ω, corresponding to the switching mode of the FE dipole. This frequency can be approximately determined if we simplify the potential energy surface U of an electric dipole to a harmonic

oscillator (inset to Fig. 2), considering only the atom that represents the moving part of the ferroelectric dipole. Assuming the atom moves along 'x' (with $P=qx$), the oscillation frequency ω can be determined to be proportional to the spring constant k based on $\omega^2 = k/m$, with $k = -\partial F/\partial x = \partial^2 U/\partial x^2$ and with $F = -\partial U/\partial x$). The dielectric response therefore shows an inverse relationship to the second derivative of the potential energy curve (Fig. 2):

$$\varepsilon \sim (\partial^2 U/\partial P^2)^{-1} \quad (3)$$

In order to extract a numerical trend for the dielectric response, let's consider a simple hypothetical ferroelectric material in an MFM configuration, of which the potential energy can be described with a simple double-well Landau potential ($U=U_0-EP+\alpha P^2+\beta P^4$ with α and β as fitting parameters) within the Gibbs-free energy framework [29]. For each value of the electric field, the polarization P is determined for which the energy U reaches a local minimum. In this local equilibrium point, Eq.(3) is then applied to estimate the dielectric response. The resulting qualitative evolution of ε is depicted in Fig. 2 and it shows a strong increase (y-axis is a multiplication factor with respect to its reference value at E=0) while approaching E_c with an electric field that can cause switching (labeled *s* in Fig. 2 and inset). Once the polarization switches, the electric field becomes a non-switching field (Fig. 2, *ns* label). For this case (Fig. 2, state 5), a decrease of ε below 2/3 of the reference value is observed.

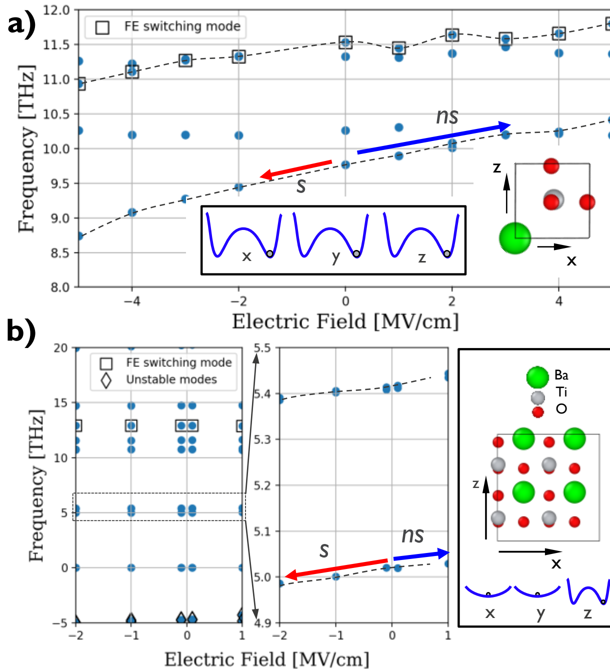

Fig. 3 Evolution of the atomic vibrational spectra under applied electric field in (a) rhombohedral and (b) tetragonal $BaTiO_3$. The 'FE switching mode' is the polarization reversal mode. Some other modes are strongly impacted by the electric field, and the corresponding points are connected with dashed lines, intended as a guide for the eye. The '*s*' labels indicate the E-fields for which switching occurs ('*ns*' for no switching E-fields). Note that the Ti atom inside the O octahedron is displaced in the[111] direction by the electric field for the rhombohedral phase (insets in a) and in the [001] direction for the tetragonal phase (insets in b). The curves show that the modes soften as switching becomes more likely.

C. First-principles predictions

To verify the qualitative picture of the analytical model, we have performed first principles dielectric response calculations. Fig. 3 depicts the DFT-computed phonon spectra for two crystalline phases of $BaTiO_3$ under applied electric field. The rhombohedral phase (ferroelectricity in the [111] direction, see insets in Fig. 3a) is chosen for the investigation since it is the stable (no imaginary soft vibrational modes) crystalline phase at the DFT temperature of 0K. The second, tetragonal phase (ferroelectricity in the [001] direction, see insets in Fig. 3b) is stable only at room temperature [30], however, we need to investigate its spectra, since the experimentally measured capacitance-voltage characteristics are collected for this phase (see next subsection). For both crystalline polymorphs, the polar modes that contribute to the dielectric response become softer (lower frequency) with a switching electric field (s-labeled/red arrow in Fig. 3) that pushes the central Ti atom in a direction that can lead to an electric polarization switch: [111] direction for the rhombohedral phase and [001] direction for the tetragonal phase. The opposite trend is valid for non-switching electric fields (ns-labeled/blue arrow in Fig. 3) – the vibrations increase in frequency and the dielectric response should drop, according to Eq.2 (Ti atom pushed against the 'potential wall' by the electric field). The phonon frequency change is originating from a change in the atomic bond stiffness with applied electric field, especially close to the coercive field.

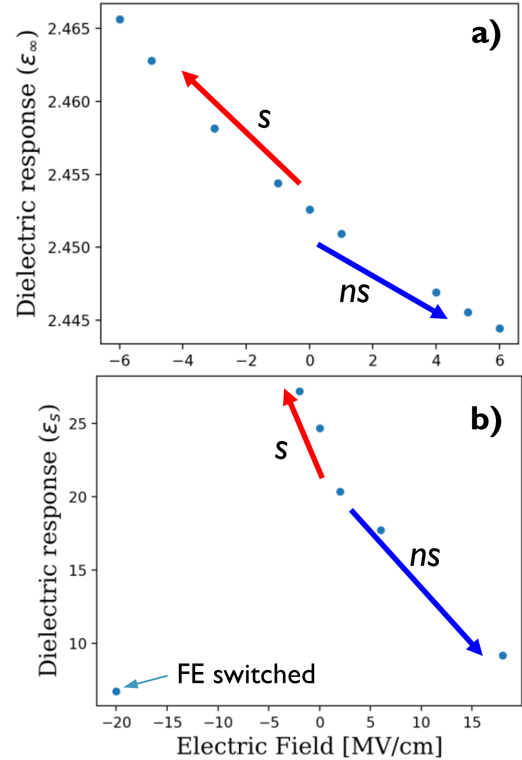

Fig. 4. (a) Electronic/optical ε_∞ component and (b) static (atomic vibrational) ε_S component of the dielectric response in r-$BaTiO_3$, computed from first principles at 0K for different electric fields. The data point at large negative fields in b) represents the ε_S value after polarization switching, and the reduced value is in agreement with the non-switching ε_S values at high positive fields.

The first-principles dielectric response is more straight-forward to compute for the stable systems (r-$BaTiO_3$), that do not show unstable/imaginary modes (as the t-$BaTiO_3$ phase does). Results are shown in Fig. 4: the dielectric response increases with switching field and decreases with non-switching fields, as expected from the vibrational frequency trends shown in Fig. 3, since the dielectric response is inversely proportional to the square of the vibrational frequencies (Eq.(2)). In Fig. 4 one can observe the same trends hold for both electronic (optical) and atomic-vibrational components of the dielectric response, though – as expected – the optical contribution is very small, compared to the atomic-vibrational component.

D. Extended NLS model

In this section we illustrate the need for a non-linear dielectric response to obtain a good agreement between the modeled and the experimentally measured C-V characteristics [31]. In particular,we implement a dielectric response model, which reflects the boost in the dielectric response close to the coercive field (Fig. 5) and which is dependent on the polarization direction of the electric dipole, with the latter determined based on the NLS model.

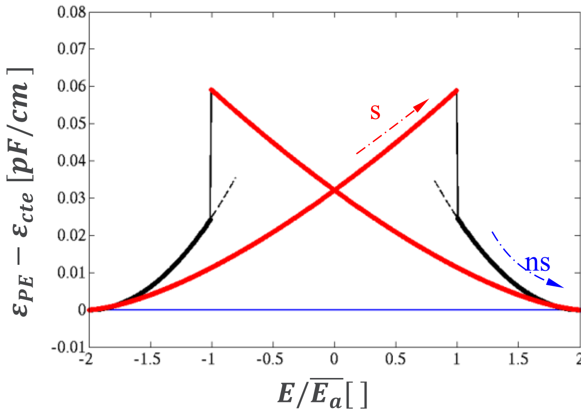

Fig. 5 Dielectric response versus normalized electric field for the default model (flat curve with $\varepsilon_{PE} = \varepsilon_{\text{cte}}$) and for the calibrated extended model (red and black curves), with the red branches corresponding to the increased dielectric response while approaching the coercive field, and with the black branches corresponding to the values immediately after a switching event.

First, using the experimental P-V data (Fig. 6a) and time-dependent response data (Fig. 6b), the default NLS model is calibrated:

$$P(t,E) = 2\,P_{\text{r}} \int_0^{\infty} \left[1 - e^{-\left(\frac{t}{\tau}\right)^n}\right] f(E_a|\overline{E_a},\sigma)\,dE_a \qquad (4)$$

with $\tau = \tau_0 e^{k.\left(\frac{E_a}{E}\right)^{\alpha}}$ and with normal distribution function $f(E_a|\overline{E_a},\sigma)$, whereby P_r is the remanent polarization, $\overline{E_a}$ the mean activation field (coercive field), σ the standard deviation of the PDF (probability density function), τ_o the intrinsic switching time and n, k and α nucleation-volume-related fitting parameters [16, 32]. The model-experiment calibration results are shown in Fig. 6(a-b) and numerical values of the parameters used are summarized in Table I. Note that the polarization value in Fig. 6b) (P_{r} = 18) is higher than in Fig. 6a) (P_{r} = 7.5) as different samples have been used (while the measurements in Fig. 6a) and 6c) have been performed on the same sample and within one measurement session). Since both samples used in Fig. 6a) and 6b) are grown on the same wafer, we assume that the time-dependent polarization evolution of both samples is sufficiently similar, such that re-use of the calibrated time-dependent data is meaningful, provided the value of P_{r} is adjusted.

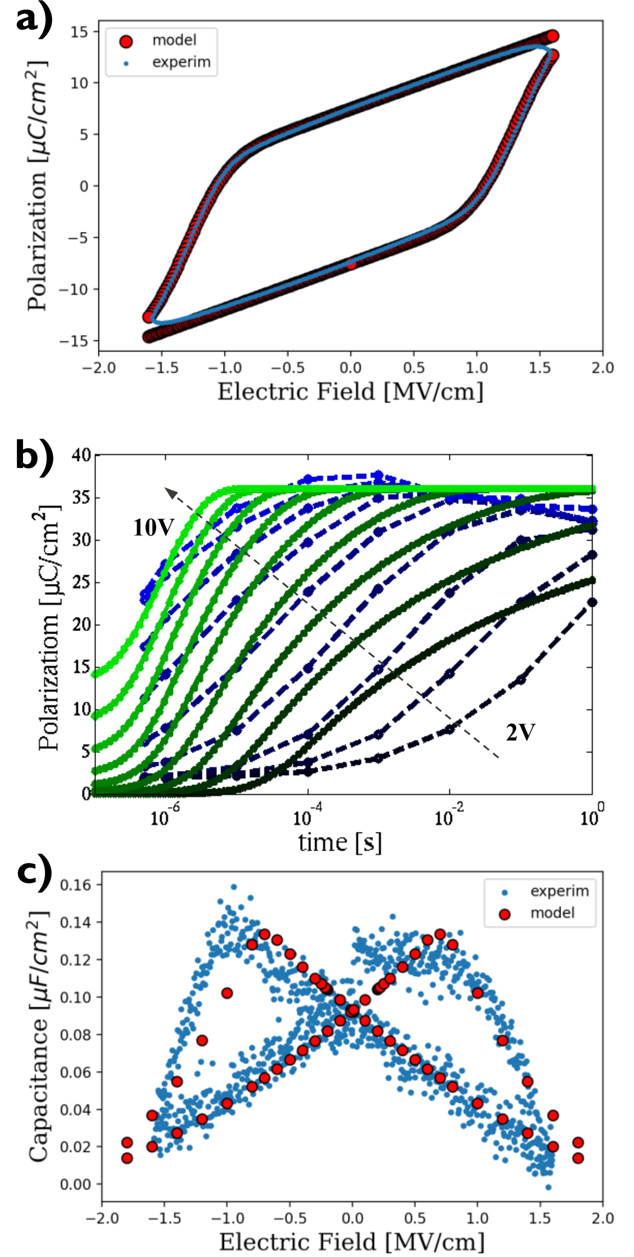

Fig. 6 a) P-V characteristics (0.5 μsec time between data points), b) time-dependent polarization measurement at different applied voltages [28] and c) C-V characteristics (1MHz small-signal freq., 10 μsec time between data points) of the $BaTiO_3$ MFM device , as measured experimentally (blue dots) and modeled by NLS with non-linear dielectric response (red circles). Note that the C-V characteristics are offset by a (constant) dielectric response of 0.55 $\mu F/cm^2$.

This NLS model is then used, together with the non-linear dielectric response (Fig. 5, with pre- and post-switching branches), to model the C-V characteristics (Fig. 6c). In this

extended NLS model, the time-dependent polarization is first determined for each domain in the multi-domain setup at each applied voltage. If the polarization of the given domain is more than 50% flipped according to the NLS model, then the post-switching dielectric response branch is used, else the pre-switching dielectric response branch is used. The dielectric response values combined with the thickness of the sample give the predictions for the C-V characteristics of the MFM sample.

The dielectric response enhancement close to switching field is able to reproduce well the experimental C-V profiles. Numerically, the change in the dielectric response, required to match the C-V characteristics of the t-$BaTiO_3$ sample, has the same order of magnitude as the ab-initio predicted values for r-$BaTiO_3$: a change of $\Delta\varepsilon_r \approx 0.3$ between $\overline{E_a}$ =1.25MV/cm and zero field is used in the extended NLS model (see Fig. 5), while first-principles calculations show an increase of $\Delta\varepsilon_r$= 2.4/(2 MV/cm) x $\overline{E_a}$ = 1.5 (see Fig. 4b) between $\overline{E_a}$ and 0 field. Note that when no dielectric response enhancement is used, no C-V matching is possible as a flat C-V characteristic is predicted with the default NLS model.

P_r []	$\overline{E_a}$ [MV/cm]	σ_{Ea} [MV/cm]	τ_o [nsec]	n []	k []	α []
a) 7.5 b) 18	1.25	0.1	1	1.5	8	0.8

Table I. Numerical values of the parameters used in the NLS model (Eq. 4).

Worth noticing, the theoretically simulated electric fields required for atomic relaxation to converge to the opposite polarization state are much higher than the typical coercive fields, measured experimentally. This is expected, since the theoretical simulations do not account for the temperature, strain effects, domain dynamics and the stochastic nature of the kinetic-barrier-crossing process, that should all decrease the electric field because of the field acceleration of the kinetic processes and that should show an electric field-switching time trade-off. While it is difficult to encompass all the phenomena that could take place in the material at the atomic level, the mere dielectric response evolution with the applied electric field can already account (at least partially) for the experimentally observed C-V behavior of the ferroelectric materials.

IV. Conclusion

In conclusion, both analytical and first-principles approaches show that the dielectric response ε in ferroelectric materials is enhanced under switching fields and inhibited under non-switching fields. This property is intrinsic to the material and due to the phonon mode softening near switching. After polarization switching, the phonon modes are hardened. The results show the limitation of using constant dielectric response values in modeling of ferroelectric materials, as they cannot account for an accurate C-V characteristic. This work adds to the understanding of the ferroelectric materials physics and advances the all-physics-based modeling of ferroelectrics.

Acknowledgments

The authors thank William G Vandenberghe for helpful discussions about the applied field in the Berry-phase approach. This work was carried out in the framework of the imec Ferroelectric Program. Financial support from EU H2020-NMBP-TO-IND-2018 Project “INTERSECT” (Grant No. 814487) is acknowledged.
Supplementary material available at https://dx.doi.org/10.21227/hb51-d608

References

[1] T. S. Boescke *et al.*, "Phase transitions in ferroelectric silicon doped hafnium oxide," *Applied Physics Letters,* vol. 99, no. 11, Sep 12 2011, Art no. 112904, doi: 10.1063/1.3636434.

[2] J. Mueller *et al.*, "Ferroelectric Zr0.5Hf0.5O2 thin films for nonvolatile memory applications," *Applied Physics Letters,* vol. 99, no. 11, Sep 12 2011, Art no. 112901, doi: 10.1063/1.3636417.

[3] J. Mueller *et al.*, "Ferroelectricity in yttrium-doped hafnium oxide," *Journal of Applied Physics,* vol. 110, no. 11, Dec 1 2011, Art no. 114113, doi: 10.1063/1.3667205.

[4] J. Mueller, T. S. Boescke, U. Schroeder, R. Hoffmann, T. Mikolajick, and L. Frey, "Nanosecond Polarization Switching and Long Retention in a Novel MFIS-FET Based on Ferroelectric HfO2," *Ieee Electron Device Letters,* vol. 33, no. 2, pp. 185-187, Feb 2012, doi: 10.1109/led.2011.2177435.

[5] S. Mueller, S. R. Summerfelt, J. Muller, U. Schroeder, and T. Mikolajick, "Ten-Nanometer Ferroelectric Si:HfO2 Films for Next-Generation FRAM Capacitors," (in English), *Ieee Electron Device Letters,* Article vol. 33, no. 9, pp. 1300-1302, Sep 2012, doi: 10.1109/led.2012.2204856.

[6] J. Mueller *et al.*, "Ferroelectricity in Simple Binary ZrO2 and HfO2," (in English), *Nano Letters,* Article vol. 12, no. 8, pp. 4318-4323, Aug 2012, doi: 10.1021/nl302049k.

[7] T. P. Ma and J. P. Han, "Why is nonvolatile ferroelectric memory field-effect transistor still elusive?," *Ieee Electron Device Letters,* vol. 23, no. 7, pp. 386-388, Jul 2002, Art no. Pii s 0741-3106(02)055349-1, doi: 10.1109/led.2002.1015207.

[8] H. Kohlstedt *et al.*, "Current status and challenges of ferroelectric memory devices," *Microelectronic Engineering,* vol. 80, pp. 296-304, Jun 2005, doi: 10.1016/j.mee.2005.04.084.

[9] X. Tian, S. Shibayama, T. Nishimura, T. Yajima, S. Migita, and A. Toriumi, "Evolution of ferroelectric HfO2 in ultrathin region down to 3 nm," (in English), *Applied Physics Letters,* Article vol. 112, no. 10, p. 5, Mar 2018, Art no. 102902, doi: 10.1063/1.5017094.

[10] E. Yurchuk *et al.*, "Impact of layer thickness on the ferroelectric behaviour of silicon doped hafnium oxide thin films," *Thin Solid Films,* vol. 533, pp. 88-92, Apr 30 2013, doi: 10.1016/j.tsf.2012.11.125.

[11] M. Popovici *et al.*, "Ferroelectric La-Doped ZrO2/HfxZr1-xO2 Bilayer Stacks with Enhanced Endurance," *Physica Status Solidi-Rapid Research Letters,* vol. 15, no. 5, May 2021, Art no. 2100033, doi: 10.1002/pssr.202100033.

[12] A. I. Khan, A. Keshavarzi, and S. Datta, "The future of ferroelectric field-effect transistor technology," *Nature Electronics,* vol. 3, no. 10, pp. 588-597, Oct 2020, doi: 10.1038/s41928-020-00492-7.

[13] M. A. Alam, M. W. Si, and P. D. D. Ye, "A critical review of recent progress on negative capacitance field-effect transistors," *Applied Physics Letters,* vol. 114, no. 9, Mar 2019, Art no. 090401, doi: 10.1063/1.5092684.

[14] D.-H. Choe *et al.*, "Surface-Functionalized Hafnia with Bespoke Ferroelectric Properties for Memory and Logic Applications," presented at the IEDM 2021.

[15] M. Sung *et al.*, "Low Voltage and High Speed 1Xnm 1T1C FE-RAM with ultra thin 5nm HZO," presented at the 2021 IEEE International Electron Devices Meeting (IEDM), 2021.

[16] A. K. Tagantsev, I. Stolichnov, N. Setter, J. S. Cross, and M. Tsukada, "Non-Kolmogorov-Avrami switching kinetics in ferroelectric thin films," *Physical Review B,* vol. 66, no. 21, Dec 2002, Art no. 214109, doi: 10.1103/PhysRevB.66.214109.

[17] C. Alessandri, P. Pandey, A. Abusleme, and A. Seabaugh, "Monte Carlo Simulation of Switching Dynamics in Polycrystalline Ferroelectric Capacitors," *Ieee Transactions on Electron Devices,*

vol. 66, no. 8, pp. 3527-3534, Aug 2019, doi: 10.1109/ted.2019.2922268.

[18] G. A. Boni *et al.*, "Low value for the static background dielectric constant in epitaxial PZT thin films," *Scientific Reports,* vol. 9, Oct 2019, Art no. 14698, doi: 10.1038/s41598-019-51312-8.

[19] S. Deng *et al.*, "Examination of the Interplay Between Polarization Switching and Charge Trapping in Ferroelectric FET," in *IEDM 2020*, 12-18 Dec. 2020, p. 4.4.1, doi: 10.1109/IEDM13553.2020.9371999.

[20] J. Hutter, M. Iannuzzi, F. Schiffmann, and J. VandeVondele, "cp2k: atomistic simulations of condensed matter systems," *Wiley Interdisciplinary Reviews: Computational Molecular Science,* vol. 4, no. 1, pp. 15-25, 2014, doi: 10.1002/wcms.1159.

[21] S. Goedecker, M. Teter, and J. Hutter, "Separable dual-space Gaussian pseudopotentials," *Physical Review B,* vol. 54, no. 3, pp. 1703-1710, Jul 1996, doi: 10.1103/PhysRevB.54.1703.

[22] J. P. Perdew, K. Burke, and M. Ernzerhof, "Generalized gradient approximation made simple," *Physical Review Letters,* vol. 77, no. 18, pp. 3865-3868, Oct 1996, doi: 10.1103/PhysRevLett.77.3865.

[23] F. Giustino, "Electron-phonon interactions from first principles," *Reviews of Modern Physics,* vol. 89, no. 1, Feb 2017, Art no. 015003, doi: 10.1103/RevModPhys.89.015003.

[24] R. Resta, "MODERN THEORY OF POLARIZATION IN FERROELECTRICS," *Ferroelectrics,* vol. 151, no. 1, pp. 49-58, 1994, doi: 10.1080/00150199408244722.

[25] R. Resta and D. Vanderbilt, "Theory of polarization: A modern approach," in *Physics of Ferroelectrics: a Modern Perspective*, vol. 105, K. M. Rabe, C. H. Ahn, and J. M. Triscone Eds., (Topics in Applied Physics, 2007, pp. 31-68.

[26] N. A. Spaldin, "A beginner's guide to the modern theory of polarization," *Journal of Solid State Chemistry,* vol. 195, pp. 2-10, Nov 2012, doi: 10.1016/j.jssc.2012.05.010.

[27] A. Togo and I. Tanaka, "First principles phonon calculations in materials science," *Scripta Materialia,* vol. 108, pp. 1-5, Nov 2015, doi: 10.1016/j.scriptamat.2015.07.021.

[28] X. Gonze and C. Lee, "Dynamical matrices, born effective charges, dielectric permittivity tensors, and interatomic force constants from density-functional perturbation theory," *Physical Review B,* Article vol. 55, no. 16, pp. 10355-10368, Apr 1997.

[29] J. Bizindavyi, A. S. Verhulst, B. Soree, and W. G. Vandenberghe, "Thermodynamic equilibrium theory revealing increased hysteresis in ferroelectric field-effect transistors with free charge accumulation," *Communications Physics,* vol. 4, no. 1, Apr 2021, Art no. 86, doi: 10.1038/s42005-021-00583-7.

[30] E. Aksel and J. L. Jones, "Advances in Lead-Free Piezoelectric Materials for Sensors and Actuators," *Sensors,* vol. 10, no. 3, pp. 1935-1954, Mar 2010, doi: 10.3390/s100301935.

[31] N. Ogata and H. Ishiwara, "A model for high frequency C-V characteristics of ferroelectric capacitors," *Ieice Transactions on Electronics,* vol. E84C, no. 6, pp. 777-784, Jun 2001.

[32] Y. Higashi *et al.*, "Investigation of Imprint in FE-HfO2 and Its Recovery," *Ieee Transactions on Electron Devices,* vol. 67, no. 11, pp. 4911-4917, Nov 2020, doi: 10.1109/ted.2020.3025846.

[33] M. N. K. Alam *et al.*, "HfZrO Ferroelectric Characterization and Parameterization of Response to Arbitrary Excitation Waveform," in *IEEE SOI-3D-Subthreshold Microelectronics Technology Unified Conference (S3S)*, San Jose, CA, Oct 14-17 2019, in IEEE SOI-3D-Subthreshold Microelectronics Technology Unified Conference, 2019, doi: 10.1109/s3s46989.2019.9320678.